Chemical Engineering Journal 413 (2021) 127477

Contents lists available at ScienceDirect

Chemical Engineering Journal

journal homepage: www.elsevier.com/locate/cej

Facile cost-effective fabrication of Cu@Cu_2O@CuO–microalgae photocatalyst with enhanced visible light degradation of tetracycline

Albert Serrà [a,*], Elvira Gómez [b,c], Johann Michler [a], Laetitia Philippe [a]

[a] Empa, Swiss Federal Laboratories for Materials Science and Technology, Laboratory for Mechanics of Materials and Nanostructures, Feuerwerkerstrasse 39, CH-3602 Thun, Switzerland
[b] Grup d'Electrodeposició de Capes Primes i Nanoestructures (GE-CPN), Departament de Ciència de Materials i Química Física, Universitat de Barcelona, Martí i Franquès, 1, E-08028 Barcelona, Catalonia, Spain
[c] Institute of Nanoscience and Nanotechnology (IN^{2}UB), Universitat de Barcelona, Barcelona, Catalonia, Spain

ARTICLE INFO

Keywords:
Photocatalysis
Antibiotics
Tetracycline
Water decontamination
Circular process
Biotemplating

ABSTRACT

The widespread use and negative environmental effects of antibiotics have made their removal from aqueous media essential in terms of wastewater treatment. Accordingly, a hybrid helical Cu@Cu_2O@CuO–microalgae photocatalyst for antibiotic photodegradation was synthesized in this study by a simple, inexpensive, and scalable process based on electroless Cu deposition and soft thermal treatment. The hybrid photocatalyst was more competitive for the photocatalytic degradation of tetracycline, especially in terms of mineralization and energy consumption, than state-of-the-art photocatalysts. The excellent photocatalytic performance is attributable to the effective formation of onion-like Cu@Cu_2O@CuO heterojunctions, which synergistically lower the electron–hole recombination rate, promote the utilization of light and photogeneration of charge carriers, and decrease the photocorrosion activity. All these effects result in the enhanced photocatalytic degradation and mineralization of tetracycline. The high photocatalytic performance of the Cu@Cu_2O@CuO–microalgae hybrids under LED irradiation resulted in a significantly lower electrical energy per order—i.e., the electrical energy required to diminish the tetracycline concentration by one order of magnitude in a unit of volume—of 57 kW h m^{-3} $order^{-1}$. Importantly, the Cu@Cu_2O@CuO–microalgae hybrids can easily be recycled after reaching their effective lifetime to fabricate competitive microalgal pellets, then integrated into a circular process in an environment–energy nexus to minimize the generation of residues.

1. Introduction

Over the past several decades, the dumping of antibiotics into ponds, canals, lakes, rivers, and other bodies of water has caused considerable concerns regarding their unknown environmental impacts and potential damage to aquatic biota [1-4]. Antibiotic drugs are continuously released into bodies of water, especially in developing countries, due to poor regulation, wastewater treatment, and management, as well as their extended use in human/veterinary medicines and agricultural production. The high levels of antibiotics in bodies of water are a leading cause for the increased multidrug resistance of microorganisms such as bacteria, viruses, fungi, and parasites that cause diseases in humans, animals, and crops [5-7]. Non-antibiotic drugs and other emerging pollutants can also increase the antibiotic resistance of microorganisms. As a result, antibiotics become ineffective in the prevention, control, treatment, and spread of infectious diseases [8-10].

Among antibiotic types, tetracyclines have long been some of the most widely used for the prevention of infectious diseases in animals and humans, thus causing many environmental issues. Tetracyclines are the second most consumed family of antibiotics in the world owing to their low cost, easy synthesis, and favorable antimicrobial activity based on the inhibition of protein synthesis [11,12]. This family of antibiotics is mainly used for the therapy and prophylaxis of human infections (e.g., atypical pneumonia, cholera, pelvic inflammations, granuloma inguinal, periodontal infection, acne vulgaris, etc.); the treatment of animal infections in veterinary medicine (e.g., poultry, sheep, swine, etc.); as animal growth promoters to improve growth rates and feed conversion efficiency, which directly translate into an important reduction in food consumption to reach marketable weight; and to control infections in aquaculture (e.g., salmon, catfish), botany (e.g., fruit trees, seeds), and

* Corresponding author.
E-mail address: a.serra@ub.edu (A. Serrà).

https://doi.org/10.1016/j.cej.2020.127477
Received 7 September 2020; Received in revised form 14 October 2020; Accepted 19 October 2020
Available online 24 October 2020
1385-8947/© 2020 The Author(s). Published by Elsevier B.V. This is an open access article under the CC BY license (http://creativecommons.org/licenses/by/4.0/).

entomoculture (e.g., honeybees) [11-13].

In this context, tetracycline (TET) has been reported as the most widely used tetracycline antibiotic in the livestock industries of many countries like the USA, China, and India due to its low cost and extensive production [5,8,10,14]. The majority of TET administered to humans and animals is incompletely metabolized, and most of the remainder (i.e., approximately 80–90%) is discharged into water environments or soil through feces and urine. Although the monitoring of TET and other antibiotics indicate that they are present in very low concentrations, from nanograms to milligrams per liter, in treated water and in high concentrations (100–800 mg L^{-1}) in hospital, pharmaceutical, and livestock wastewater, the alarming increase in the antimicrobial resistance of microorganisms mandates that the removal of antibiotics in water be included in decontamination technology [8,15-18]. The global trends in the antimicrobial resistance of animals evidence the influence of livestock industries, as drug-resistant microorganisms are gaining a stronghold in regions such as India, China, Kenya, Uruguay, and Brazil, where meat production has risen sharply since 2000 [10]. The development of intensive farming practices based on the administration of antibiotics, including TET, to promote growth and prevent infections, as well as lenient legislation and poor wastewater treatment, are critical for understanding these global trends [10,16,19,20].

Due to the potential risks of antibiotics, the development of efficient and cost-effective strategies for their removal is urgent. The removal of TET and its metabolites from aqueous environments is complicated due to their low biodegradability, high stability, and structural complexity. Various methods have been tested for the removal of TET such as biodegradation, biofiltration, electrochemical oxidation, membrane filtration, adsorption, and advanced oxidation processes like photocatalytic degradation [9,21-25]. Of these, adsorption and photocatalytic processes have been noted as the most effective strategies due to the amphoteric nature and multiple functional groups (e.g., phenol, alcohol) of TET, which facilitate its adsorption onto adsorbents or photocatalyst surfaces. However, there remains a need for appropriate adsorbents and efficient photocatalysts that can easily be integrated into wastewater plants and reused for real applications [21,22,26].

In this work, a facile, mass-productive, green, and cost-effective method for the fabrication of a hybrid helical Cu@Cu_2O@-CuO–microalgae photocatalyst with enhanced visible-light-driven mineralization of TET was developed. The process holistically integrates the principles of green and circular chemistry, minimizing waste and increasing the efficiency of the use of energy, water, and chemicals [27-29]. The circular process begins and ends in the cultivation of microalgae (more specifically, *Spirulina platensis*), which have significant potential for the fixation of carbon dioxide (i.e., the compound produced by the complete photooxidation of TET) and other residues that are generated throughout the process (i.e., copper-rich ashes) [29,30]. Importantly, the cultivation of microalgae results in the net release of large amounts of molecular oxygen into the atmosphere. Furthermore, the cultivated microalgae can be used for multiple applications, including biofuel production and cosmetics [30,31]. The Cu@Cu_2O@CuO–microalgae photocatalyst was synthesized by a simple two-step biotemplating process based on the electroless deposition of Cu onto the surface of microalgae and subsequent controlled formation of an onion-like Cu@Cu_2O@CuO multilayered architecture by annealing. The formation of Cu/Cu_2O/CuO heterojunctions resulted in an exceptional photocatalytic performance for mineralizing TET under white light-emitting diode (LED) irradiation. The possibility of using LED technology significantly reduces the energy consumption, simplifying the integration of the photocatalyst into photo-reactors. The mechanisms of the photodegradation, photostability, and reusability of the photocatalysts were investigated. This work contributes to the fabrication of efficient, recyclable, green, and low-cost core@shell@shell Cu@Cu_2O@CuO–microalgae photocatalysts to replace today's linear "take–make–dispose" thinking with circular processes with the final aim of facilitating the applicability of photocatalysts to water decontamination.

2. Experimental

2.1. Synthesis and characterization of Cu@Cu_2O@CuO-microalgae photocatalyst

Arthrospira platensis cyanobacteria (axenic strain, Strain No. NIVA-CYA 428) were used as a biotemplate for the cost-effective production of the hybrid helical Cu@Cu_2O@CuO–microalgae photocatalyst. The cyanobacteria were cultivated in Zarrouk's medium (pH = 9.8) in an open-air tank at 30.0 ± 0.4 °C under natural sunlight irradiation [27]. The synthesis of the hybrid helical Cu@Cu_2O@CuO–microalgae photocatalyst was based on a two-step method (Scheme 1):

(i) *Electroless deposition of Cu*: The microalgae were collected using a nylon mesh filter and directly subjected to a Pd catalyzation process. No expensive or time-consuming fixation process was employed during biotemplating. The filtered microalgae were dispersed in a Pd catalyzation bath, which consisted of stannous chloride and palladium chloride colloidally dispersed in a dilute solution of sulfuric acid and sodium chloride, for 35 min at 35 °C. During this process, Pd nuclei were formed on the microalgae, which catalyze the electroless deposition of Cu from a copper electroless bath. After Pd surface functionalization, the microalgae were added to an electroless plating solution and maintained under magnetic stirring (400 rpm) at 40.0 ± 0.6 °C for 120 min to deposit Cu onto their surface. The electroless plating solution consisted of copper(II) sulphate (0.04 M), potassium sodium tartrate (0.05 M), disodium ethylenediaminetetraacetate dihydrate (0.07 M), formaldehyde (1 M), thiourea (1.3 μM), and sodium hydroxide (0.25 M). The electroless plating solution was prepared and its pH was adjusted to 12 immediately before the addition of the catalyzed microalgae. After electroless Cu deposition, the metalized microalgae were separated by filtration using a nylon mesh filter, washed thoroughly with water and ethanol, and finally completely dried in air. After drying, the metalized microalgae were placed on a glass plate [32,33].

(ii) *Controlled oxidation of Cu*: The dried metallic microalgae were annealed at 200 °C for 8 h in an air atmosphere at a heating rate of 5 °C min^{-1}. The annealing treatment was performed using rapid thermal annealing equipment (Advanced Riko Mila 5050). After the annealing process, the formation of the hybrid helical Cu@Cu_2O@CuO–microalgae photocatalyst was expected.

Different characterization techniques were used to confirm the formation and properties of the hybrid helical Cu@Cu_2O@CuO–microalgae photocatalyst. A field emission scanning electron microscope (FE-SEM; Hitachi, S-4800) equipped with an energy-dispersive X-ray spectrometer (EDX) was used to analyze the morphology of the microalgae surfaces after the biotemplating process and to confirm the deposition of Cu. The elemental composition was also estimated by X-ray fluorescence (Fischer, Fischerscope X-RAY XDV-SDD). The architectures of both the bare and metallized microalgae were examined by optical microscopy (Zeiss, AxioMat), and the crystallinity and microstructure were determined by X-ray diffraction (XRD; Bruker, D8 Discovery diffractometer) in the Bragg–Brentano configuration with CuK_α radiation. The specific surface area of the photocatalyst was determined based on the Brunauer–Emmett–Teller (BET) method from N_2 adsorption–desorption isotherms measured at 77 K using a Micrometrics Tristar-II. The chemical states of the photocatalyst were examined by X-ray photoelectron spectroscopy (XPS; Physical Electronics, PHI 5600 Multitechnique) using a monochromatic X-ray source (Al K_α line = 1486.6 eV, 350 W). The photocatalyst was etched by argon ion sputtering up to a few nanometers prior to acquiring the angle-resolved XPS spectra. The optoelectronic properties of the photocatalyst were analyzed by the UV–vis

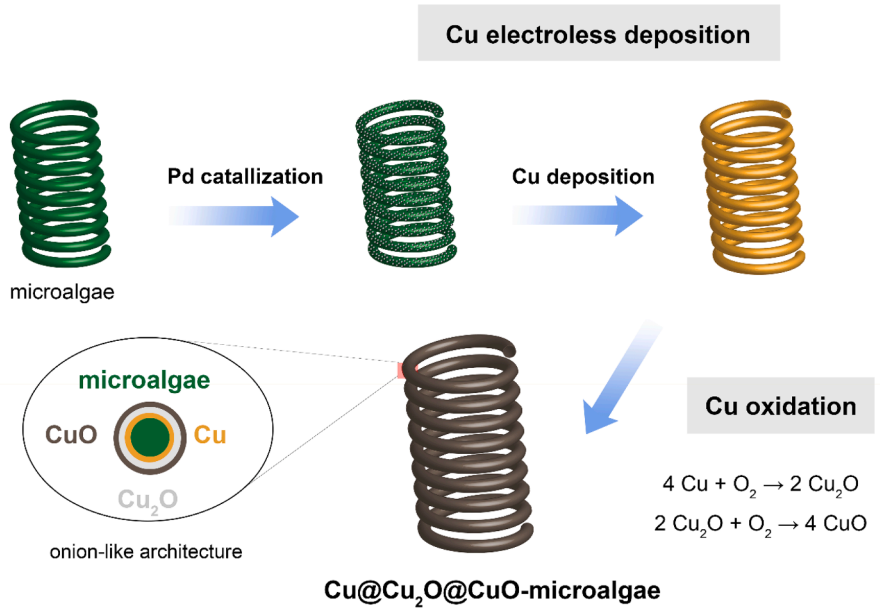

Scheme 1. Schematic illustration of the Cu@Cu_2O@CuO–microalgae hybrid photocatalyst synthesis.

diffuse reflectance spectra (DRS) obtained with a UV–vis spectrophotometer (PerkinElmer, Lambda 900 UV).

2.2. Degradation and mineralization of tetracycline

The adsorption experiments were carried out in dark conditions at room temperature (25 ± 1 °C) to determine the time required to reach the adsorption–desorption equilibrium of TET (Alfa Aesar) on our photocatalyst. The adsorption process was investigated at pH 6 and 8. In a typical experiment, 250 mg of helical Cu@Cu_2O@CuO–microalgae was suspended in 500 mL of a TET solution (40 mg L^{-1}) and maintained under constant magnetic stirring (500 rpm) in dark conditions. At given time points during the experiment, 2.5 mL of the suspension was removed and filtered using a 0.45 μm cellulose acetate syringe membrane filter. Afterward, the TET content in the supernatant was measured by UV–vis spectrophotometer (Lambda 900 UV, λ = 362 nm). All experiments were performed in quadruplicate.

The photocatalytic removal of TET was performed in 500-mL solution consisting of 0.5 g L^{-1} Cu@Cu_2O@CuO–microalgae and 40 mg L^{-1} TET. The suspension was maintained at 25 ± 1 °C and subjected to magnetic stirring (500 rpm) before and during irradiation, and the initial pH was adjusted with NaOH (1.0 M) or HCl (1.0 M) prior to the addition of the photocatalyst. Before irradiation began, the suspension was kept in the dark at 25 ± 1 °C until the system reached adsorption–desorption equilibrium. Controlled irradiation of the suspension was performed using three 6.2 W LEDs (luminous flux = 575 lm; energy consumption = 7 kWh (1000 h)); Figure S1 depicts the relative intensity as a function of wavelength. Photolytic experiments (without the photocatalyst) were conducted to consider the photolytic degradation of TET during 80 min of exposure to the three 6.2 W white LEDs. The photocatalytic experiments were conducted at pH = 6 and 8. The photocatalytic degradation of TET was measured according to the temporal evolution of the reduction in the maximum absorption peak intensity of TET (362 nm) under LED irradiation for 80 min using a UV–vis spectrophotometer (Shimadzu, UV-1800) in a quartz cuvette with an optical path length of 1 cm. During the photocatalytic degradation experiments, the major intermediate products in the degraded TET solution were determined by liquid chromatography-mass spectroscopy (LC-MS, Waters Xevo G2-XS QToF) analysis. The mineralization was calculated by measuring the reduction in total organic carbon (TOC) after 120 and 180 min under LED irradiation, by the high-temperature combustion method using TOC-V_{CSH} equipment (Shimadzu) with a high-sensibility column. All samples were subjected to filtration through a 0.22 μm nylon membrane filter prior to determination of the TET content, intermediates or TOC. All experiments were performed in quadruplicate.

To determine the role of the reactive oxygen species generated during the photocatalytic process, free radical trapping experiments were performed via the addition of selective radical scavengers. For this purpose, isopropyl alcohol (IPA; Sigma-Aldrich, >99.7%) as a quencher of hydroxyl radicals, benzoquinone (BQ; Sigma-Aldrich, >99.7%) as a quencher of superoxide radicals, and triethanolamine (TEOA; Sigma-Aldrich, >99%) as a quencher of photogenerated holes were used. In these experiments, the radical scavengers were independently added to separate experiments to attain a concentration of 1 mM. Next, after reaching adsorption–desorption equilibrium in dark conditions at 25 ± 1 °C under magnetic stirring (500 rpm), the suspensions were irradiated using the three 6.2 W LEDs for 120 min. Finally, the concentration of TET was measured according to the maximum absorption peak intensity of TET (362 nm) using a UV–vis spectrophotometer (UV-1800). The trapping experiments were performed at pH 6 and 8. All experiments were performed in quadruplicate. To further confirm the existence of hydroxyl and superoxide radical's electron spin resonance (ESR) experiments in 5,5-dimethyl-1-pyrroline-N-oxide (DMPO) were performed with a Bruker A200-9.5/12 spectrometer in the dark and under LED visible light irradiation.

2.3. Reusability and photostability of Cu@Cu_2O@CuO–microalgae photocatalyst

The reusability and photostability of the Cu@Cu_2O@CuO–microalgae photocatalyst were evaluated by measuring the photodegradation efficiency of a 40 mg L^{-1} TET solution for 10 consecutive cycles under LED irradiation. The photocatalyst stability after this reusability experiment was evaluated in terms of BET surface area and FE-SEM morphological analysis. The long-term stability of the Cu@Cu_2O@CuO–microalgae was evaluated by measuring the Cu(II) concentration every day for 4 d of exposure to the three 6.2 W LEDs. The suspensions were maintained at 25 ± 1 °C under magnetic stirring (500 rpm) during the irradiation period. The photostability of the photocatalyst was examined at pH = 6 and 8. The concentration of Cu ions was determined by a spectrophotometric method using a thiomichlersketone (>85.0%) and using a UV–vis spectrophotometer (UV-1800) [34]. All

experiments were performed in quadruplicate.

3. Results and discussion

3.1. Synthesis and characterization of $Cu/Cu_2O/CuO$-microalgae photocatalyst

The microalgae hybrid photocatalyst consisted of *A. platensis*, which acts as a structural support, covered with an onion-like $Cu@Cu_2O@CuO$ multilayered shell. Under the employed cultivation conditions, the average dimensions of the *A. platensis* microhelices (Figure S2) were a wire diameter of 4–7 μm, helix diameter of 18–24 μm, and length of 70–100 μm (5–9 turns). It is known that the shape and average dimensions of *A. platensis* microhelices can be tuned by varying the cultivation conditions, like the temperature, light intensity, and cultivation environment [27,32,33].

The onion-like $Cu@Cu_2O@CuO$–microalgae hybrid photocatalyst was synthesized by a simple biotemplating process based on (i) copper electroless deposition, which generates a smooth Cu metallic layer (>95% in content), followed by (ii) a copper oxidation process via a simple annealing treatment at 200 °C for 8 h in an air atmosphere [35]. Importantly, no time-consuming and expensive fixation of *A. platensis* is required in our method. The electroless process begins with Pd catalyzation, involving the formation and adsorption of Pd nuclei onto the *A. platensis* surfaces, which subsequently catalyze the deposition of metallic Cu from the copper electroless plating bath to completely cover the microalgae surfaces and result in the formation of Cu–microalgae hybrids. These hybrids were annealed in air, resulting first in the formation of a Cu_2O layer on their surface, which in turn protected the inner Cu layer and simultaneously acted as a precursor to grow CuO via a vapor–solid mechanism [35-37]. This process resulted in the fabrication of the $Cu@Cu_2O@CuO$–microalgae hybrid photocatalyst.

As shown in Figure S2, the green microalgae turned dark gray after the electroless plating and annealing processes. Importantly, although no microalgae fixation was performed, a process that is normally used to avoid fragmentation, the hybrid photocatalyst kept the initial shape of *A. platensis*, and the microhelices were unbroken. FE-SEM (Fig. 1) and EDX spectroscopic observations confirmed the formation of the $Cu@Cu_2O@CuO$–microalgae hybrid photocatalyst. As shown in Fig. 1, the hybrids maintained the original microhelical shape of the microalgae. Although the electroless process did not affect the architecture of the microalgae, it did result in a significantly higher surface roughness (Figure S3). A similar rough morphology has also been observed during the electroless deposition of other metals onto the surface of fixed microalgae [27,33]. The surface morphology was typically rough, and no obvious morphological changes were observed after the annealing process. The average dimensions of the $Cu@Cu_2O@CuO$–microalgae hybrids were a wire diameter of 6–9 μm, helix diameter of 19–26 μm, and length of 70–100 μm (5–9 turns). The thickness of the coating on the surface of the *A. platensis* was estimated as approximately 1 μm. Importantly, the $Cu@Cu_2O@CuO$–microalgae hybrids can be considered lightweight photocatalysts since sedimentation was practically negligible during 10 h of non-stirring conditions.

*Fig. 2a shows the XRD patterns of the non-annealed hybrids (i.e., Cu–microalgae hybrids; curve i) and the hybrids annealed at 200 °C for 8 h in an air atmosphere (i.e., $Cu@Cu_2O@CuO$–microalgae hybrids; curve ii). The XRD pattern of the as-synthesized Cu–microalgae hybrids exhibited three clear peaks at $2\theta = 43.3°$, 50.3°, and 74.1°, which were indexed to the (111), (200), and (220) reflections, respectively, of the pure face-centered cubic structure of Cu (JCPDS No. 04–0836). No evidence of CuO, Cu_2O, or $Cu(OH)_2$ was found. However, after the annealing treatment, new diffraction peaks appeared that perfectly matched the cubic-phase crystal structure of cuprite (JCPDS No. 05–0667) and monoclinic crystal structure of tenorite (JCPDS No. 89–5898). The peaks at $2\theta = 29.9°$, 36.4°, 42.3°, and 61.4° were indexed to the (110), (111), (200), and (220) reflections of Cu_2O (JCPDS No. 05–0667), respectively, and those at $2\theta = 36.1°$, 38.6°, 48.6°, 58.1°, 61.4°, and 65.9° were indexed to the (−111), (111), (−202), (020), (−113), and (022) reflections of the CuO phase (JCPDS No. 89–5898), respectively. No other phases were detected after the annealing treatment. Higher temperatures were detrimental to the integrity of the hybrid architecture as the bioorganic skeleton of the microalgae began to undergo calcination.

Fig. 2b shows the nitrogen adsorption–desorption isotherm of the $Cu@Cu_2O@CuO$–microalgae hybrids. The BET surface area of the hybrids was 138 $m^2\ g^{-1}$, which is significantly higher than that of the dried microalgae powder (90.3 $m^2\ g^{-1}$). The higher BET of the hybrids is attributable to the high surface roughness of the $Cu@Cu_2O@CuO$ coating, which may be beneficial for heterogeneous catalytic purposes.

XPS analysis was used to further investigate the elemental chemical states of Cu and O in the $Cu@Cu_2O@CuO$ heterojunctions. The binding energies obtained from the XPS analysis were corrected for specimen charging by referencing the C 1 s peak to 284.60 eV. As shown in Fig. 2c, the high-resolution Cu 2p spectrum consisted of two main asymmetric

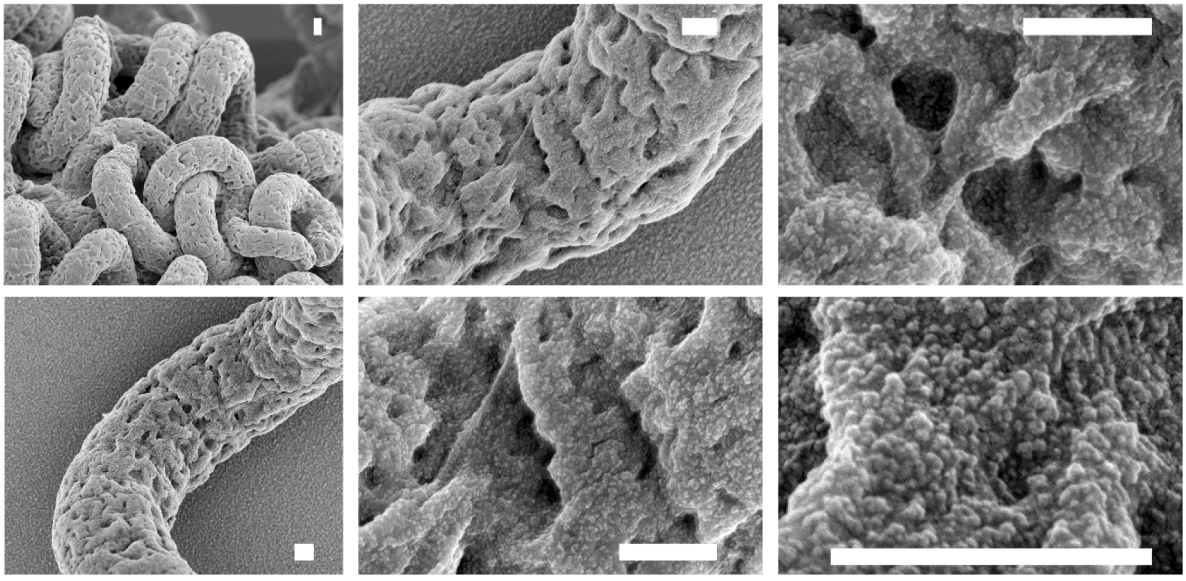

Fig. 1. FE-SEM micrographs of the $Cu@Cu_2O@CuO$–microalgae photocatalyst. Scale bar: 1 μm.

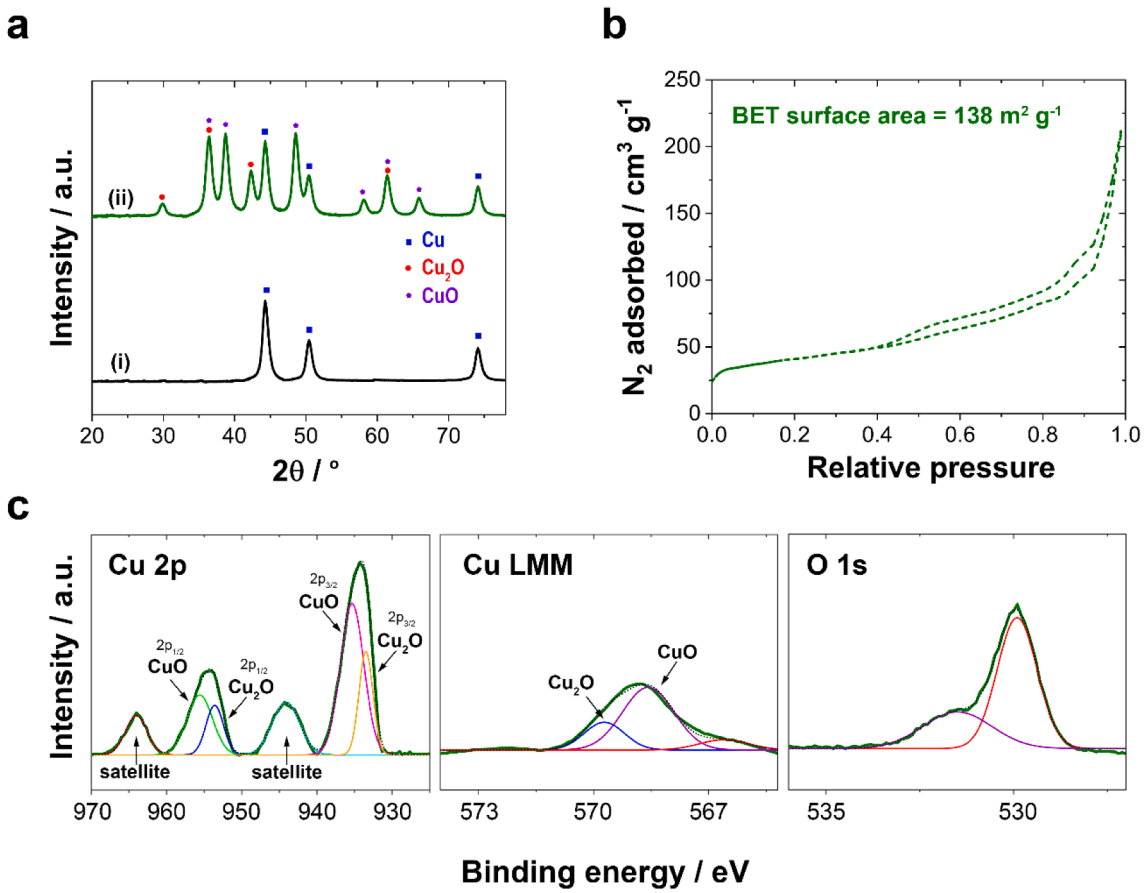

Fig. 2. (a) XRD patterns of the (i) Cu–microalgae hybrids and (ii) Cu@Cu_2O@CuO–microalgae hybrids. (b) Nitrogen adsorption–desorption isotherm and (c) XPS spectra of the Cu@Cu_2O@CuO–microalgae hybrids.

peaks centered at 954.3 and 934.1 eV, which correspond to Cu $2p_{1/2}$ and Cu $2p_{3/2}$, respectively, accompanied by two extra peaks centered at 964.0 and 944.1 eV attributable to the satellite peaks of Cu_2O and CuO, respectively. The two main peaks were deconvoluted into four peaks at 953.5 and 933.5 eV corresponding to Cu $2p_{1/2}$ and Cu $2p_{3/2}$ of Cu^+, respectively, which verified the existence of Cu_2O, and 955.6 and 935.3 eV corresponding to Cu $2p_{1/2}$ and Cu $2p_{3/2}$ of CuO, respectively [35,38,39]. The Cu LMM Auger peaks located at 569.7 and 568.6 eV, which were assigned to Cu^+ and Cu^{2+}, respectively, also are consistent with the formation of Cu/Cu_2O/CuO heterojunctions consisting of an onion-like core@shell@shell Cu@Cu_2O@CuO architecture. The O 1 s region exhibited a clear asymmetric peak that was deconvoluted into two peaks centered at 531.5 and 529.9 eV. The main peak at 529.9 eV was ascribed to lattice oxygen from both the Cu_2O and CuO phases, while the peak at 531.5 eV is related to surface hydroxyl groups [35,38,39].

The EDX, XRD, and XPS analyses clearly proved the presence of Cu, Cu_2O, and CuO on the surface of microalgae after the biotemplating process, but these results alone give no information about their arrangement. However, the idea of the formation of Cu@Cu_2O@-CuO–microalgae hybrids in an onion-like arrangement is reinforced by the formation mechanism based on the autocatalytic deposition of Cu followed by its superficial thermal oxidation, resulting first in the formation of a superficial layer of Cu_2O, that in turn protects the inner Cu layer and acts as a precursor for the formation of CuO.

As shown in Fig. 3, the optical properties of the Cu@Cu_2O@-CuO–microalgae hybrids were investigated by UV–vis DRS to understand the effect of the Cu_2O/CuO heterojunctions on light absorption. The bandgap energies of pure Cu_2O and CuO are 2.2 and 1.7 eV, respectively, and the corresponding bandgap energy of the

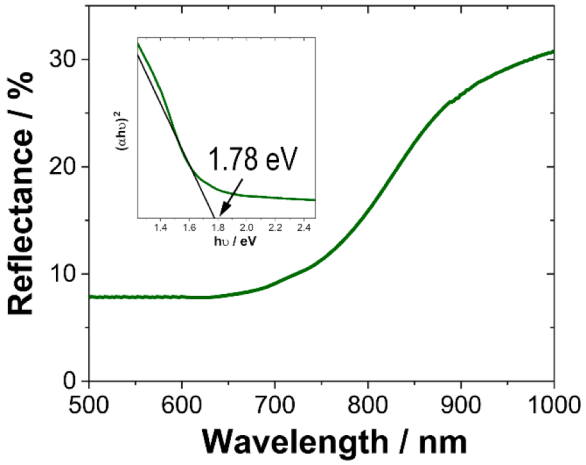

Fig. 3. UV–vis DRS of Cu@Cu_2O@CuO–microalgae hybrids (inset: Tauc plot from the UV–vis analysis).

Cu@Cu_2O@CuO–microalgae hybrids calculated by the transformed Kubelka–Munk function was 1.78 eV [35,40-42]. The microalgae architecture and formation of Cu_2O/CuO heterojunctions translated into enhanced photo-absorption, which might result in a higher photoactivity.

3.2. Degradation and mineralization of TET

The photocatalytic performance of the Cu@Cu_2O@CuO–microalgae hybrids was determined by photocatalytically degrading TET in an

aqueous solution under visible LED irradiation [9,43,44]. The photolytic and photocatalytic degradation of TET were carried out at pH 6.0 and 8.0. At pH = 6.0, the dominant TET species is the zwitterionic form (i.e., equal number of positively and negatively charged functional groups), whereas at pH = 8.0, the primary species is negatively charged [45-47]. Note that the point of zero charge of the Cu@Cu_2O@CuO–microalgae hybrids is approximately 9.3. Thus, at pH < 9.3, the surface charge of the Cu@Cu_2O@CuO–microalgae hybrids is mainly positive; at pH ≈ 9.3, the surface is neutral; and at pH > 9.3, the surface charge is predominantly negative [35,38]. The speciation of TET and the surface charge of the photocatalyst are governed by the solution pH, which may have an important influence on photolytic and photocatalytic degradation. In addition, copper oxides, especially Cu_2O, dissolve well under acidic conditions (pH < 5). It is not recommended to employ copper-oxides-based photocatalysts in acidic or weakly acidic conditions; instead, the ideal operational pH range at ambient temperatures is from 7 to 10 for Cu_2O and 8 to 11 for CuO, where dissolution is practically negligible [48,49]. Therefore, considering both the surface charge and solubility of copper oxide based photocatalysts, the speciation of TET, and the normal pH of wastewater, the photocatalytic degradation of TET was investigated at pH = 6.0 and 8.0.

The adsorption of TET species by the Cu@Cu_2O@CuO–microalgae hybrids was investigated in dark conditions. As shown in Fig. 4a, the system quickly reached adsorption–desorption equilibrium within 40 min in dark conditions at pH = 6.0 and 8.0. Importantly, the interaction capacity of the Cu@Cu_2O@CuO–microalgae hybrids was significantly higher at pH = 8.0 (19.1%) than at pH = 6.0 (6.1%) (Figure S4). This can be attributed to the fact that the Cu@Cu_2O@CuO–microalgae hybrid surfaces remain positively charged in this pH range, which enables the electrostatic attraction of not only negatively charged TET species (pH = 8.0) but also the zwitterionic species (pH = 6.0). The improved electrostatic interaction performance at pH = 8.0 is expected to result in enhanced photocatalytic degradation. In dark conditions and in the absence of the photocatalyst, the degradation of TET was negligible. The photolytic degradation of TET was also investigated in the absence of photocatalysts. At pH = 6.0, only a small amount (<1.2%) of TET was degraded after 4 h under LED irradiation, whereas the photolytic degradation at pH = 8.0 was significantly higher (<3%). Thus, the photolytic degradation of TET was enhanced by increasing the pH.

As shown in Fig. 4b, the photocatalytic degradation of TET under LED irradiation strongly depended on the solution pH. The results showed that 98.3% and 76.5% of the TET was photocatalytically degraded after 80 min of LED irradiation at pH = 8.0 and 6.0, respectively. This can be attributed to both the higher adsorption of TET onto the photocatalyst surface and the greater absorption of light by TET molecules at pH = 8.0. The photocatalytic degradation kinetics were investigated according to the Langmuir–Hinshelwood model. As shown in Fig. 4b, the photocatalytic degradation behavior complied with the pseudo-first-order kinetic model. The kinetic rate constants were estimated as 5.01 × 10^{-2} min^{-1} (4.0 × 10^{-1} min^{-1} g^{-1}) and 1.83 × 10^{-2} min^{-1} (1.5 × 10^{-1} min^{-1} g^{-1}) at pH 8.0 and 6.0, respectively. These photocatalytic TET degradation rates for the Cu@Cu_2O@CuO–microalgae hybrids are similar to or even higher than those of the most competitive state-of-the-art photocatalysts (Table 1) [18,22,44,50-

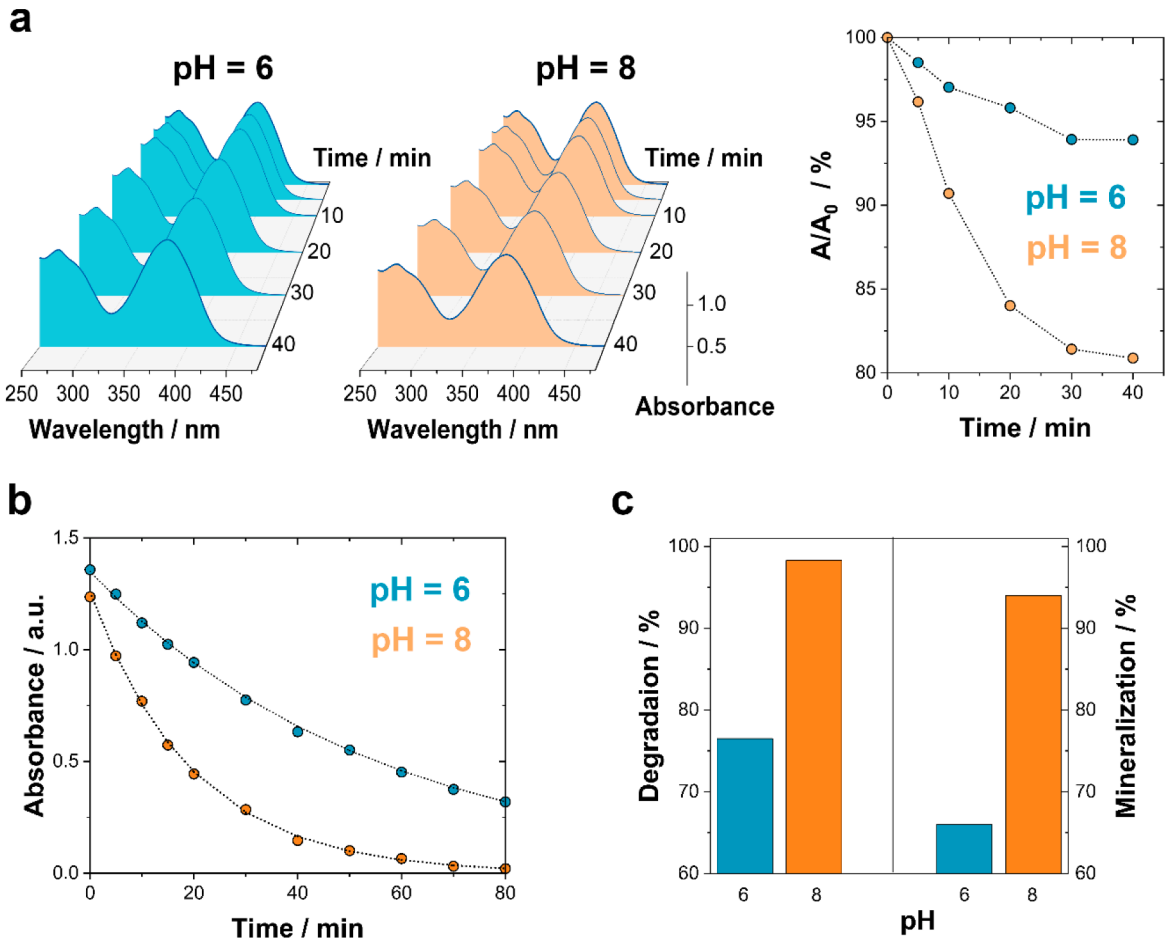

Fig. 4. (a) Time-dependent UV–vis spectra of TET adsorption in dark conditions using 0.5 g L^{-1} Cu@Cu_2O@CuO–microalgae hybrids. (b) Photocatalytic degradation of TET (40 mg L^{-1}) under LED irradiation using 0.5 g L^{-1} Cu@Cu_2O@CuO–microalgae hybrids. (c) Photocatalytic degradation (80 min) and mineralization (120 min) of TET (40 mg L^{-1}) using 0.5 g L^{-1} Cu@Cu_2O@CuO–microalgae hybrids after 80 and 120 min of LED irradiation, respectively.

59]. More importantly, the energy consumption, which is directly associated with the cost of the photocatalytic treatment, is markedly less than that of state-of-the-art photocatalysts due to the use of LED light and the excellent photocatalytic performance of the Cu@Cu_2O@-CuO–microalgae hybrids. As shown in Table 1, the electrical energy per order (E_{EO})—i.e., the electric energy required to diminish the TET concentration by one order of magnitude in a unit of volume—of this system at pH = 8.0 is 57 kW h m^{-3} $order^{-1}$, which is much lower (18–700 times) than that of other systems and reactor configurations [18,22,44,50-59]. Note that the E_{EO} parameter cannot be solely attributed to the photocatalyst nature as some of the aspects of E_{EO} are intrinsic to the reactor configuration. However, it can be used to compare different systems regardless of the experimental setup. This is extremely important since the viability of photocatalytic water treatment lies largely in the energy costs.

LC-MS was used to further investigate the photocatalytic degradation of TET at pH = 8.0. The major intermediates generated during the photocatalytic degradation of TET were identified to explore the photocatalytic degradation pathway. As shown in Figure S5, 13 major compounds appeared during the irradiation process. The intensity of the characteristic peak of TET (m/z = 445) decreased gradually with increasing irradiation time, indicating its degradation. During the irradiation process, new peaks were detected at m/z = 447, 431, 417, 362, 340, 329, 319, 283, 227, 149, 120, 118, 100, and 91. A plausible TET photocatalytic degradation pathway was proposed based on the detected emerging molecules. As shown in Fig. 5, the proposed pathway starts via the demethylation of an amino group (position 2). The small peak at m/z = 363 may be ascribable to deamination and dehydroxylation reactions. The peaks at m/z = 340, 319, and 283 may be due to dehydroxylation, whereas the peak at m/z = 329 is likely caused by the removal of methyl, amino, and hydroxyl groups. The peaks at m/z = 149, 120, 118, 100, and 91 are potentially caused by the cleavage of carbon–carbon bonds and ring-opening reactions. In order to evaluate if the intermediates were completely mineralized into carbon dioxide, water, and eco-friendly inorganic species, the TOC was also determined after the irradiation process.

The mineralization of TET by the Cu@Cu_2O@CuO–microalgae under LED irradiation was evaluated by TOC measurements. As shown in Fig. 4c, a>90% (pH = 8.0) and 60% (pH = 6.0) decrease in TOC of the TET solutions was observed after 120 min of irradiation. These are lower than the TET degradation values, which indicated that the photocatalytic mineralization of TET occurred via many complex steps. Moreover, the mineralization was also enhanced at a higher pH. The total mineralization of TET (>99%) was confirmed after 180 min of irradiation at pH = 8.0, whereas a greater mineralization time was needed at pH = 6.0. Importantly, the mineralization activity of the Cu@Cu_2O@CuO–microalgae hybrids is also equal to or higher than that of state-of-the-art photocatalysts (Table 1) [18,22,44,50-59]. Therefore, the Cu@Cu_2O@CuO–microalgae hybrids offer an excellent photocatalytic mineralization performance under LED irradiation in addition to their economic competitivity.

The role of the main active photogenerated species (i.e., hydroxyl radicals, superoxide radicals, and photogenerated holes) involved in the photodegradation process was investigated through free radical trapping experiments to explore the photodegradation mechanism of the Cu@Cu_2O@CuO–microalgae hybrids. In this experiment, 1 mM TEOA, BQ, or IPA solutions were employed as a scavenger of holes (h^+), superoxide radicals ($^{\bullet}O_2^-$), or hydroxyl radicals ($^{\bullet}OH$), respectively. As shown in Fig. 6a, at pH = 8, the photocatalytic degradation (98.3%) of TET using the Cu@Cu_2O@CuO–microalgae hybrids after 80 min of LED irradiation decreased to 18%, 48%, and 8% in the presence of the hole, superoxide radical, and hydroxyl radical scavengers, respectively. The same trend was observed at pH = 6. These results suggested that the photogenerated holes and especially the hydroxyl radicals governed the photocatalytic degradation of TET when the Cu@Cu_2O@-CuO–microalgae hybrids were used as photocatalysts.

To further confirm the role of hydroxyl and superoxide radicals in the photocatalytic degradation of TET under LED visible light irradiation, ESR spin-trapping experiments were performed. As shown in Fig. 6b and 6c, no obvious signals corresponding to the DMPO-$^{\bullet}OH$ and DMPO-$^{\bullet}O_2^-$ adducts were detected in dark conditions. However, after 5 min of irradiation, the characteristic quadruple signal with a relative signal ratio of 1:2:2:1, corresponding to the DMPO-$^{\bullet}OH$ adduct emerged under visible-light irradiation. Importantly, the signal intensities gradually increased with irradiation time (Fig. 6b). The characteristic signal of $^{\bullet}O_2^-$ with a relative signal ratio of 1:1:1:1also appeared and increased in intensity with visible light irradiation time, but it was weaker than the $^{\bullet}OH$ signal. Based on these results, which indicate an abundance of $^{\bullet}OH$ radicals, $^{\bullet}OH$ radicals govern the photooxidation of TET, whereas $^{\bullet}O_2^-$ only partially contributes to TET oxidation.

Based on the above experimental results, a possible TET photodegradation mechanism for the Cu@Cu_2O@CuO–microalgae hybrids under visible LED irradiation was proposed (Fig. 6d). According to the literature, pure Cu_2O and CuO are photosensitive in the visible domain due to their narrow bandgaps (2.2 and 1.7 eV, respectively) [35,42,62]. However, the relatively rapid recombination of electron–hole pairs and high photocorrosion rate hinder their potential use in photocatalytic applications. Knowledge of the relative band edge positions of the Cu@Cu_2O@CuO–microalgae hybrid photocatalyst is crucial to clarify the improved photocatalytic performance. The band edge positions of the valence band (VB) and conduction band (CB) of CuO and Cu_2O can be determined using the following equation (Eq. (1)):

$$E_{CB}^{0} = \chi - E^{c} - \frac{1}{2}E_{g} \quad (1)$$

where χ is the Mulliken absolute electronegativity (5.81 and 6.85 eV for CuO and Cu_2O, respectively), E^c is the energy of free electrons on the hydrogen scale (i.e., 4.5 eV), and E_g is the band gap of the semiconductor [35,42]. The predicted band edge positions for CuO and Cu_2O are summarized in Table 2.

As shown in Fig. 6b, the bandgap positions of Cu_2O and CuO facilitate interfacial charge transfer in the Cu/Cu_2O/CuO heterojunctions. The excited electrons in the CB of Cu_2O can shift to the CB of CuO or be accepted by the conductive metallic Cu core, while the holes photoproduced by CuO are transferred to the VB of Cu_2O. This phenomenon results in the effective separation of electron–hole pairs. Therefore, the transfer and separation of electron–hole pairs in the Cu/Cu_2O/CuO heterojunctions could significantly hinder their recombination and consequently improve the photocatalytic performance [42,62]. The electrons in the CB of CuO can react with adsorbed oxygen molecules, leading to the formation of superoxide radicals. On the other hand, the holes in the VB can react with adsorbed water or hydroxyl ions to form hydroxyl radicals or with TET molecules to form smaller molecules, or directly transform small adsorbed organic molecules into CO_2 and H_2O. The hydroxyl radicals are mainly generated via the reaction of photogenerated holes with the adsorbed water and hydroxyl ions since the other possible sources, like the reaction of superoxide radicals with protons or the photolysis of water, are less prevalent in neutral and alkaline media [27,35,63]. In conclusion, the formation of Cu/Cu_2O/CuO heterojunctions leads to an enhanced photocatalytic performance due to a reduced recombination process. In addition, the formation of these heterojunctions also improves the photocorrosion resistance (see section 3.3) [27,63]. Therefore, the Cu@Cu_2O@CuO–microalgae hybrids exhibited an improved photocatalytic performance that is relevant to the challenge of real applicability to photocatalytic water treatment.

3.3. *Reusability and photostability of Cu@Cu_2O@CuO–microalgae photocatalyst*

The photostability and reusability of photocatalysts are pivotal factors for their applicability in photocatalytic water treatment. According to the literature, the formation of Cu/Cu_2O/CuO heterojunctions not

Table 1
Operational conditions and photocatalytic performance for TET photodegradation.

Photocatalyst	Photocatalyst dosage / g L^{-1}	TET / g L^{-1}	pH	Volume / mL	Light source	Treatment time / min	Degradation / %	Kinetic constant / min^{-1}	Mineralization (time) / %	Electrical energy per order (E_{EO}) / kW h m^{-3} $order^{-1}$	Reference
Cu/Cu_2O/CuO-microalgae	0.5	0.040	6	250	3 LEDs (6.2 W)	80	76.5	0.0183	66 (120 min)	156	This work
Cu/Cu_2O/CuO-microalgae	0.5	0.040	8	250	3 LEDs (6.2 W)	80	98.3	0.0501	94 (120 min)	57	This work
BiOI microspheres	1.0	0.040	n.a.	50	Xe lamp (1000 W)	240	94	0.0198	73 (240 min)	12,921	[22]
TiO_2 P-25	1.0	0.040	9	40	UV (300 W)	60	95	n.a.	60 (60 min)	n.a.	[18]
MWNTs-Bi_2WO_6	0.5	0.020	11	50	Xe lamp (800 W)	60	83	0.0295	n.a.	27,752	[17]
CNS-TiO_2	0.5	0.005	9	250	Xe lamp (150 W)	180	97	0.0210	26 (180 min)	1,096	[54]
In_2S_3@MIL-125(Ti)	0.3	0.046	5.9	100	Xe lamp (300 W)	60	63	0.0167	17 (60 min)	6,894	[53]
CDs/g-C_3N_4/MoO_3	0.6	0.020	n.a.	50	Xe lamp (350 W)	90	88	0.0231	n.a.	11,629	[55]
AgI/$BiVO_4$	0.3	0.020	n.a.	100	Xe lamp (300 W)	60	95	0.0547	91 (60 min)	2,105	[44]
BiOI/Ag@AgI	0.3	0.020	n.a.	100	Xe lamp (300 W)	60	86	0.0317	48 (60 min)	3,631	[56]
Ag/Bi_3TaO_7	n.a.	0.010	n.a.	n.a.	Xe lamp (250 W)	60	86	0.0390	n.a.	n.a.	[57]
Ag/Ag_2CO_3/$BiVO_4$	0.4	0.020	n.a.	50	Xe lamp (500 W)	150	83	0.0186	n.a.	11,004	[13]
MWCNT/TiO_2	0.2	0.010	5.0	200	2 UVC lamps (6 W)	60	98	0.0640	83 (300 min)	48	[60]
Ag_3PO_4/$CuBi_2O_4$	0.5	0.010	n.a.	100	Xe lamp (300 W)	60	75	0.0201	n.a.	7,637	[58]
Ag/$AgIn_5S_8$	0.3	0.010	4.5	100	Xe lamp (300 W)	240	93	0.0111	56.3 (540 min)	3,457	[59]
$SrTiO_3$/$MnFe_2O_4$	1.0	0.022	n.a.	20	Hg lamp (200 W)	25	68.5	0.0868	n.a.	14,148	[50]
Polyaniline/perylene diimide	0.5	0.020	5.0	50	LED (5 W)	120	65	0.0088	40.1 (120 min)	437	[51]
$BiVO_4$/$FeVO_4$@rGO	0.6	0.030	n.a.	50	Xe lamp (1000 W)	100	91.5	0.0247	n.a.	24,859	[61]
AgI/UiO-66(NH_2)	0.3	0.010	6.0	100	Xe lamp (300 W)	40	81	0.0360	66 (40 min)	6,396	[52]

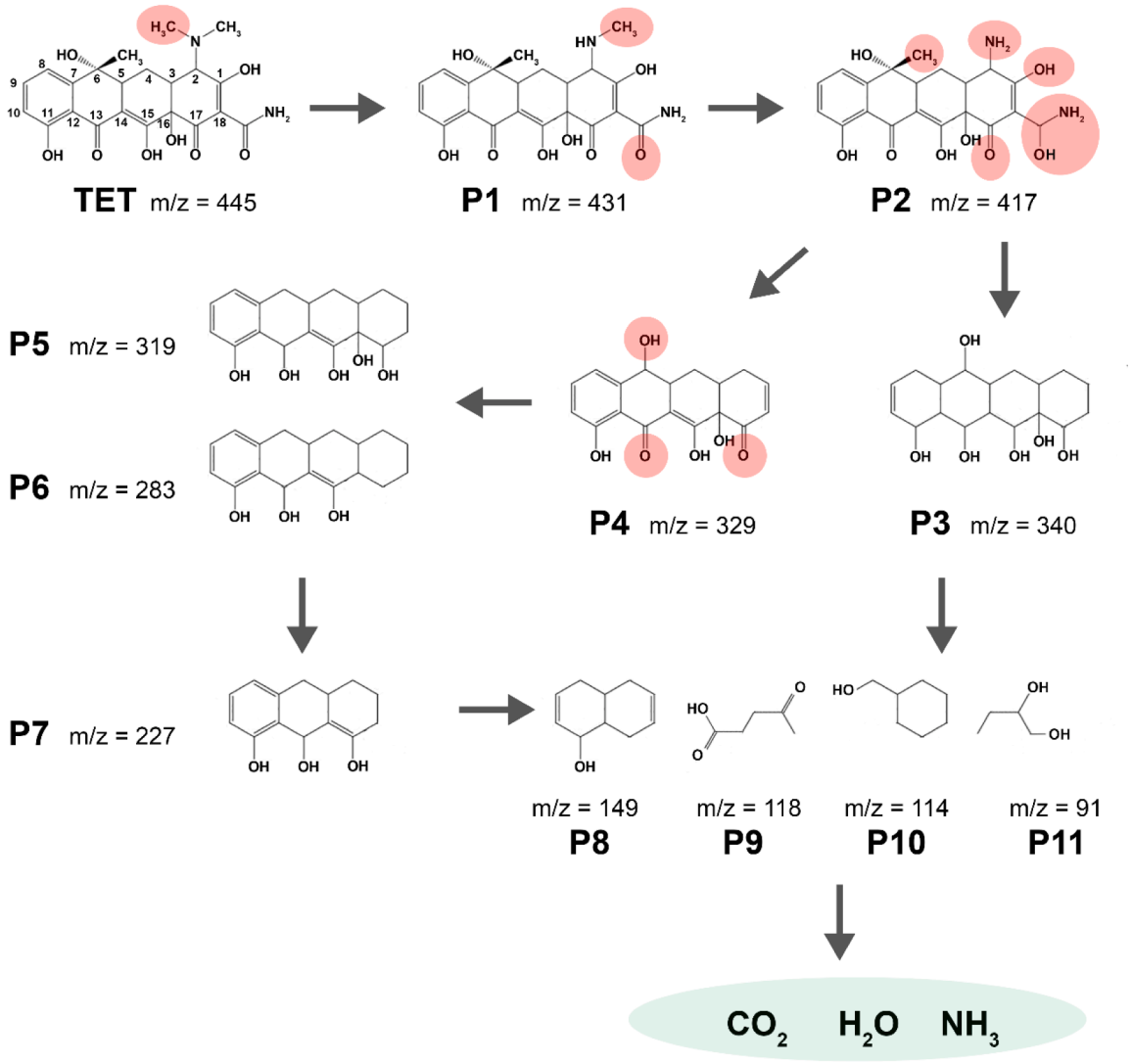

Fig. 5. Possible photocatalytic degradation pathway of TET.

only improves the photostability of copper-oxide-based photocatalysts, primarily by preventing photocorrosion, but also critically hinders their relatively strong electron–hole pair recombination. Note that an important limitation of using copper oxides in photocatalytic water treatment is the relatively high photocorrosion activity of Cu_2O and CuO [41,64-66]. As shown in Fig. 7a, the Cu@Cu_2O@CuO–microalgae hybrids exhibited excellent reusability, as the level of photocatalytic degradation remained nearly constant across 10 consecutive experiments at both pH = 6.0 and 8.0. The high stability of the Cu@Cu_2O@-CuO–microalgae hybrids was reflected by the high and stable photocatalytic turnover numbers (TONs). The calculated TONs of the Cu@Cu_2O@CuO–microalgae hybrids achieved in 10 consecutive cycles were approximately 480 and 620 for pH = 6.0 and 8.0, respectively. Importantly, these experiments did not affect the catalyst surface morphology (Fig. 7b). The BET surface areas measured after the reusability experiments were 136 and 139 $m^2\ g^{-1}$ for the Cu@Cu_2O@-CuO–microalgae hybrids used at pH = 6.0 and 8.0, respectively. The XRD, XPS, and EDS analyses after the reusability experiments (Figure S6) compared with those of the as-prepared photocatalysts elucidated the high stability of these hybrids. Thus, the formation of a Cu/Cu_2O/CuO heterojunction seems to have significantly hindered the two known photocorrosion pathways of Cu_2O (i.e., Cu_2O self-photoreduction into Cu metal by photo-generated electrons and self-photooxidation into CuO by photo-induced holes). This outcome may be attributable to the promoted transfer of electrons and holes to the surface of CuO and Cu_2O, respectively, which facilitates external photochemical reactions (Fig. 6d) that minimize the Cu_2O self-photooxidation and self-photoreduction [67].

To further investigate the stability of the Cu@Cu_2O@-CuO–microalgae hybrids, the time-dependent concentration of Cu ions in the aqueous solution was spectroscopically determined over 120 h under LED irradiation. As shown in Fig. 8, the Cu@Cu_2O@-CuO–microalgae hybrids displayed excellent resistance to chemo- and photocorrosion at both pH = 6.0 and 8.0, with photocatalyst dissolutions of<6% and 3%, respectively. Even so, the stability improved at pH = 8.0, the lowest reported point of solubility for Cu_2O. Because Cu_2O is unstable in both acidic and basic conditions [48,67], the formation of a Cu/Cu_2O/CuO heterojunction also improved the chemical stability of Cu_2O by virtue of its protective outer layer of CuO. Ultimately, after 120 h of continuous irradiation, no structural or morphological damage was observed with FE-SEM.

Finally, based on a recently published paper from our group, the fabrication of microalgae pellets (i.e., biofuel for combustion) was proposed to recycle the photocatalyst upon reaching its effective lifetime [30]. Microalgal pellets satisfy the requirements for consideration as commercial biofuels according to the ISO 17225–6:2014 standard for non-woody pellets. In turn, the microalgal ashes resulting from the combustion of these recycled microalgal pellets can be used for water

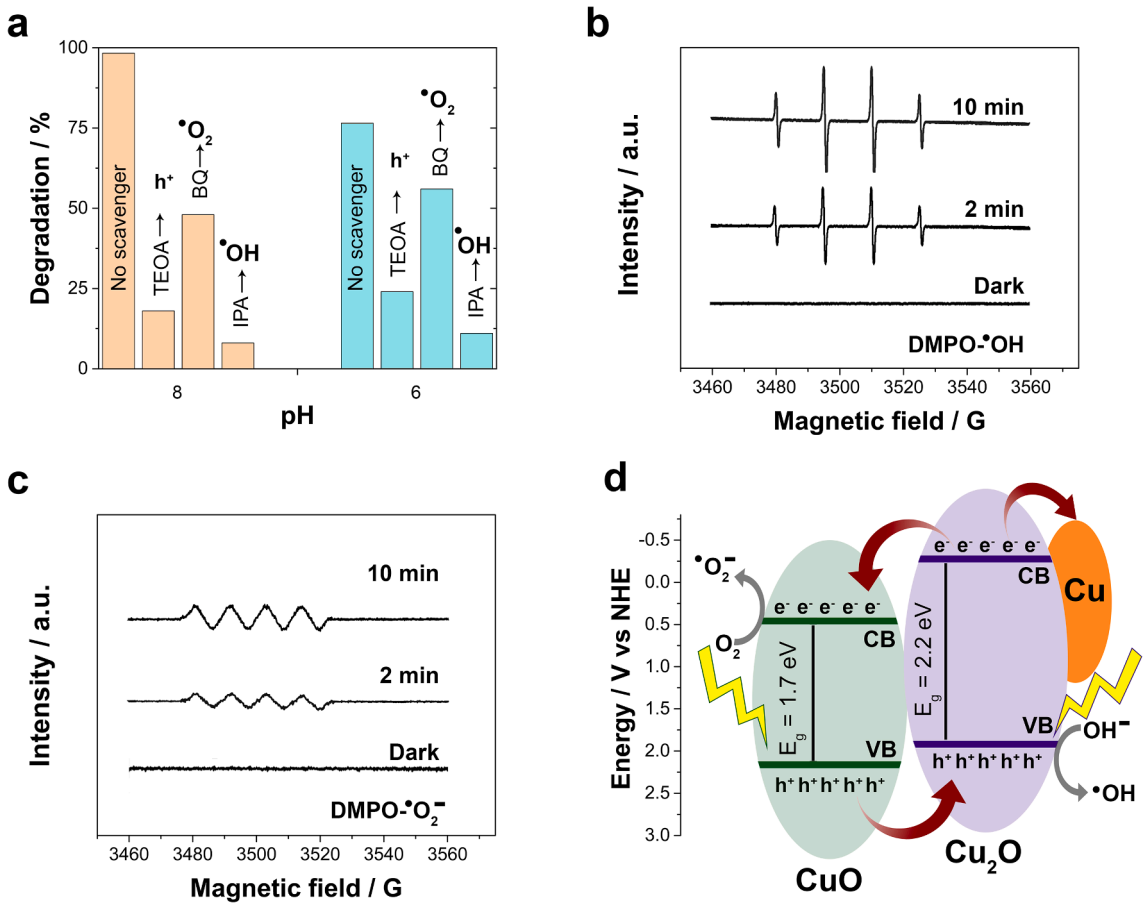

Fig. 6. (a) Trapping of active species during TET photocatalytic degradation under LED irradiation using the Cu@Cu_2O@CuO–microalgae hybrids (0.5 g L^{-1}) during 80 min. ESR spectra of (b) DMPO-$^{\bullet}$OH and (c) DMPO-$^{\bullet}O_2^-$ in the dark and under LED visible light irradiation. (d) Schematic representation of the photocatalytic mechanism of the Cu@Cu_2O@CuO–microalgae hybrids.

Table 2
Mulliken absolute electronegativity, band gap energy, calculated CB edges, and calculated VB edges of CuO and Cu_2O.

Semiconductor	χ	E_g / eV	CB edge / eV	VB edge / eV
CuO	5.81	1.7	0.46	2.16
Cu_2O	5.32	2.2	−0.28	1.92

decontamination and/or as a supplement for microalgae cultivation [29,31]. Therefore, the Cu@Cu_2O@CuO–microalgae hybrids offer an excellent photocatalytic performance owing to their nature, optoelectronic properties, reduced recombination rate, high photocorrosion resistance, and potential recyclability after their effective lifetime. Consequently, they can be integrated into circular processes to increase the efficiency of the use of energy, water, resources, residues, and human capital.

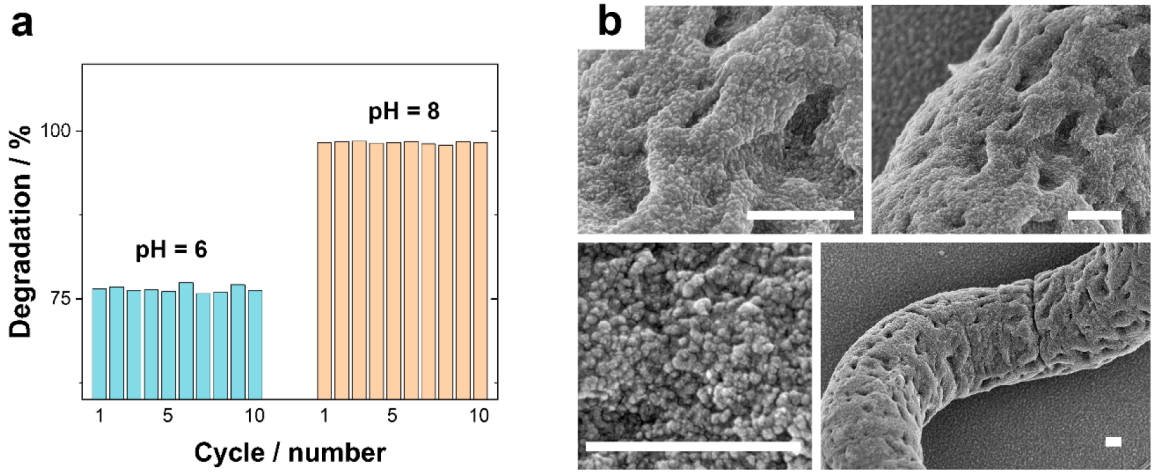

Fig. 7. (a) Photocatalytic degradation ratio (80 min) of TET (40 mg L^{-1}) using 0.5 g L^{-1} Cu@Cu_2O@CuO–microalgae hybrids under LED irradiation for 10 reusability cycles. (b) FE-SEM micrographs of Cu@Cu_2O@CuO–microalgae hybrids after use for 10 reusability cycles. Scale bar: 1 μm.

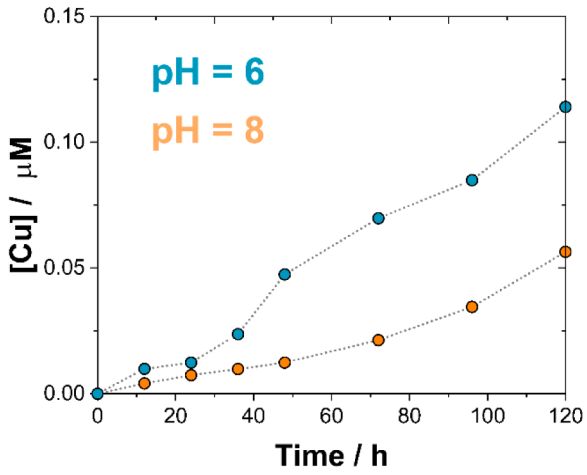

Fig. 8. Time-dependent concentration of Cu ions in an aqueous solution under LED irradiation in the presence of 0.5 g L^{-1} Cu@Cu_2O@-CuO–microalgae hybrids.

4. Conclusions

A hybrid Cu@Cu_2O@CuO–microalgae photocatalyst was synthesized using simple and scalable electroless deposition and thermal treatment processes. This simple biotemplating approach is a more scalable process than other physical methods for fabricating well-defined microhelices. It is known that microhelical architectures are beneficial in terms of light absorption, pollutant adsorption, and suspension in aqueous media. Moreover, the use of a microalgae skeleton allows for recycling of the Cu@Cu_2O@CuO–microalgae photocatalysts after their effective lifetime to produce microalgal pellets, which can then be used as a supplement for microalgae cultivation media, thus offering a circular process to reduce/eliminate the generation of residues.

The formation of onion-like Cu@Cu_2O@CuO heterojunctions not only improves the photocatalytic performance, which principally derives from the synergistic effects between the three materials, but also lowers the electron–hole recombination rate, which promotes the utilization of light and the photogeneration of charge carriers, and reduces the photocorrosion activity. As a result, the formation of heterojunctions effectively addresses two major setbacks to the use of copper oxides as photocatalysts in water decontamination —the relatively high recombination rate of electron–holes pairs and the photocorrosion of Cu_2O. The excellent performance of the Cu@Cu_2O@CuO–microalgae photocatalyst for the photocatalytic degradation of TET as a representative antibiotic is markedly more competitive than that of state-of-the-art photocatalysts due to the rapid mineralization and low E_{EO} from the use of LED irradiation. The outstanding photocatalytic performance of the photocatalyst in TET photocatalytic degradation and its chemo- and photostability from pH = 6.0 to 8.0—the usual pH range of wastewater containing TET— reinforces its applicability in technologies for decontaminating real water.

Declaration of Competing Interest

The authors declare that they have no known competing financial interests or personal relationships that could have appeared to influence the work reported in this paper.

Acknowledgements

This work was supported by the Metrohm foundation. Albert Serrà would like to acknowledge funding from the EMPAPOSTDOCS-II program. The EMPAPOSTDOCS-II programme has received funding from the European Union's Horizon 2020 research and innovation programme under the Marie Skłodowska-Curie grant agreement number 754364.

Appendix A. Supplementary data

Supplementary data to this article can be found online at https://doi.org/10.1016/j.cej.2020.127477.

References

[1] F. Baquero, J.L. Martínez, R. Cantón, Antibiotics and antibiotic resistance in water environments, Curr. Opin. Biotechnol. 19 (2008) 260–265, https://doi.org/10.1016/j.copbio.2008.05.006.
[2] P. Verlicchi, M. Al Aukidy, E. Zambello, Occurrence of pharmaceutical compounds in urban wastewater: Removal, mass load and environmental risk after a secondary treatment-A review, Sci. Total Environ. 429 (2012) 123–155, https://doi.org/10.1016/j.scitotenv.2012.04.028.
[3] M.D. Hernando, M. Mezcua, A.R. Fernández-Alba, D. Barceló, Environmental risk assessment of pharmaceutical residues in wastewater effluents, surface waters and sediments, Talanta. 69 (2006) 334–342, https://doi.org/10.1016/j.talanta.2005.09.037.
[4] J.L. Martinez, Environmental pollution by antibiotics and by antibiotic resistance determinants, Environ. Pollut. 157 (2009) 2893–2902, https://doi.org/10.1016/j.envpol.2009.05.051.
[5] D. Wang, F. Jia, H. Wang, F. Chen, Y. Fang, W. Dong, G. Zeng, X. Li, Q. Yang, X. Yuan, Simultaneously efficient adsorption and photocatalytic degradation of tetracycline by Fe-based MOFs, J. Colloid Interface Sci. 519 (2018) 273–284. doi: 10.1016/j.jcis.2018.02.067.
[6] H. Wang, Y. Wu, M. Feng, W. Tu, T. Xiao, T. Xiong, H. Ang, X. Yuan, J.W. Chew, Visible-light-driven removal of tetracycline antibiotics and reclamation of hydrogen energy from natural water matrices and wastewater by polymeric carbon nitride foam, Water Res. 144 (2018) 215–225, https://doi.org/10.1016/j.watres.2018.07.025.
[7] Y. Wang, S. Gong, Y. Li, Z. Li, J. Fu, Adsorptive removal of tetracycline by sustainable ceramsite substrate from bentonite/red mud/pine sawdust, Sci. Rep. 10 (2020) 1–18, https://doi.org/10.1038/s41598-020-59850-2.
[8] J. Hou, W. Wan, D. Mao, C. Wang, Q. Mu, S. Qin, Y. Luo, Occurrence and distribution of sulfonamides, tetracyclines, quinolones, macrolides, and nitrofurans in livestock manure and amended soils of Northern China, Environ. Sci. Pollut. Res. 22 (2015) 4545–4554, https://doi.org/10.1007/s11356-014-3632-y.
[9] A. Cai, J. Deng, M. Xu, T. Zhu, S. Zhou, J. Li, G. Wang, X. Li, Degradation of tetracycline by UV activated monochloramine process: Kinetics, degradation pathway, DBPs formation and toxicity assessment, Chem. Eng. J. 395 (2020), 125090, https://doi.org/10.1016/j.cej.2020.125090.
[10] T.P. Van Boeckel, J. Pires, R. Silvester, C. Zhao, J. Song, N.G. Criscuolo, M. Gilbert, S. Bonhoeffer, R. Laxminarayan, Global trends in antimicrobial resistance in animals in low- And middle-income countries, Science 80- (2019)). 365, https://doi.org/10.1126/science.aaw1944.
[11] C. Ian, R. Marilyn, Tetracycline Antibiotics: Mode of Action, Applications, Molecular Biology, and Epidemiology of Bacterial Resistance, Microbiol. Mol. Biol. Rev. 65 (2001) 232–260, https://doi.org/10.1128/MMBR.65.2.232.
[12] A.A. Borghi, M.S.A. Palma, Tetracycline: Production, waste treatment and environmental impact assessment, Brazilian J. Pharm. Sci. 50 (2014) 25–40, https://doi.org/10.1590/S1984-82502011000100003.
[13] Y. Liu, J. Kong, J. Yuan, W. Zhao, X. Zhu, C. Sun, J. Xie, Enhanced photocatalytic activity over flower-like sphere Ag/Ag2CO3/BiVO4 plasmonic heterojunction photocatalyst for tetracycline degradation, Chem. Eng. J. 331 (2018) 242–254, https://doi.org/10.1016/j.cej.2017.08.114.
[14] N. Moullan, L. Mouchiroud, X. Wang, D. Ryu, E.G. Williams, A. Mottis, V. Jovaisaite, M.V. Frochaux, P.M. Quiros, B. Deplancke, R.H. Houtkooper, J. Auwerx, Tetracyclines disturb mitochondrial function across eukaryotic models: A call for caution in biomedical research, Cell Rep. 10 (2015) 1681–1691, https://doi.org/10.1016/j.celrep.2015.02.034.
[15] Y. Zhou, X. Liu, Y. Xiang, P. Wang, J. Zhang, F. Zhang, J. Wei, L. Luo, M. Lei, L. Tang, Modification of biochar derived from sawdust and its application in removal of tetracycline and copper from aqueous solution: Adsorption mechanism and modelling, Bioresour. Technol. 245 (2017) 266–273, https://doi.org/10.1016/j.biortech.2017.08.178.
[16] X. Zhu, Y. Liu, C. Zhou, G. Luo, S. Zhang, J. Chen, A novel porous carbon derived from hydrothermal carbon for efficient adsorption of tetracycline, Carbon N. Y. 77 (2014) 627–636, https://doi.org/10.1016/j.carbon.2014.05.067.
[17] L. Yue, S. Wang, G. Shan, W. Wu, L. Qiang, L. Zhu, Novel MWNTs-Bi2WO6 composites with enhanced simulated solar photoactivity toward adsorbed and free tetracycline in water, Appl. Catal. B Environ. 176–177 (2015) 11–19, https://doi.org/10.1016/j.apcatb.2015.03.043.
[18] X.D. Zhu, Y.J. Wang, R.J. Sun, D.M. Zhou, Photocatalytic degradation of tetracycline in aqueous solution by nanosized TiO2, Chemosphere. 92 (2013) 925–932, https://doi.org/10.1016/j.chemosphere.2013.02.066.
[19] A. De, J. Sosa, D.K. Byarugaba, C.F. Amabile-Cuevas, P.R. Hsueh, S. Kariuki, I. N. Okeke, Antimicrobial resistance in developing countries, Antimicrob. Resist. Dev. Ctries. (2010) 1–554, https://doi.org/10.1007/978-0-387-89370-9.

[20] J.A. Ayukekbong, M. Ntemgwa, A.N. Atabe, The threat of antimicrobial resistance in developing countries: Causes and control strategies, Antimicrob. Resist. Infect. Control. 6 (2017) 1–8, https://doi.org/10.1186/s13756-017-0208-x.

[21] H.R. Pouretedal, N. Sadegh, Effective removal of Amoxicillin, Cephalexin, Tetracycline and Penicillin G from aqueous solutions using activated carbon nanoparticles prepared from vine wood, J. Water Process Eng. 1 (2014) 64–73, https://doi.org/10.1016/j.jwpe.2014.03.006.

[22] R. Hao, X. Xiao, X. Zuo, J. Nan, W. Zhang, Efficient adsorption and visible-light photocatalytic degradation of tetracycline hydrochloride using mesoporous BiOI microspheres, J. Hazard. Mater. 209–210 (2012) 137–145, https://doi.org/10.1016/j.jhazmat.2012.01.006.

[23] H. Qin, H. Cheng, H. Li, Y. Wang, Degradation of ofloxacin, amoxicillin and tetracycline antibiotics using magnetic core–shell MnFe2O4@C-NH2 as a heterogeneous Fenton catalyst, Chem. Eng. J. 396 (2020), 125304, https://doi.org/10.1016/j.cej.2020.125304.

[24] X.R. Jing, Y.Y. Wang, W.J. Liu, Y.K. Wang, H. Jiang, Enhanced adsorption performance of tetracycline in aqueous solutions by methanol-modified biochar, Chem. Eng. J. 248 (2014) 168–174, https://doi.org/10.1016/j.cej.2014.03.006.

[25] L. Hou, L. Wang, S. Royer, H. Zhang, Ultrasound-assisted heterogeneous Fenton-like degradation of tetracycline over a magnetite catalyst, J. Hazard. Mater. 302 (2016) 458–467, https://doi.org/10.1016/j.jhazmat.2015.09.033.

[26] A.C. Martins, O. Pezoti, A.L. Cazetta, K.C. Bedin, D.A.S. Yamazaki, G.F.G. Bandoch, T. Asefa, J.V. Visentainer, V.C. Almeida, Removal of tetracycline by NaOH-activated carbon produced from macadamia nut shells: Kinetic and equilibrium studies, Chem. Eng. J. 260 (2015) 291–299, https://doi.org/10.1016/j.cej.2014.09.017.

[27] A. Serrà, R. Artal, J. García-Amorós, B. Sepúlveda, E. Gómez, J. Nogués, L. Philippe, Hybrid Ni@ZnO@ZnS-Microalgae for Circular Economy: A Smart Route to the Efficient Integration of Solar Photocatalytic Water Decontamination and Bioethanol Production, Adv. Sci. 7 (2020) 1–9, https://doi.org/10.1002/advs.201902447.

[28] T. Keijer, V. Bakker, J.C. Slootweg, Circular chemistry to enable a circular economy, Nat. Chem. 11 (2019) 190–195, https://doi.org/10.1038/s41557-019-0226-9.

[29] A. Serrà, R. Artal, J. García-Amorós, E. Gómez, L. Philippe, Circular zero-residue process using microalgae for efficient water decontamination, biofuel production, and carbon dioxide fixation, Chem. Eng. J. 388 (2020), 124278, https://doi.org/10.1016/j.cej.2020.124278.

[30] A. Serrà, P. Pip, E. Gómez, L. Philippe, Efficient magnetic hybrid ZnO-based photocatalysts for visible-light-driven removal of toxic cyanobacteria blooms and cyanotoxins, Appl. Catal. B Environ. 268 (2020) 118745. doi:10.1016/j.apcatb.2020.118745.

[31] R. Artal, L. Philippe, E. Gómez, A. Serrà, Recycled cyanobacteria ashes for sono-enhanced photo-Fenton wastewater decontamination, J. Clean. Prod. 267 (2020), https://doi.org/10.1016/j.jclepro.2020.121881.

[32] K. Kamata, Z. Piao, S. Suzuki, T. Fujimori, W. Tajiri, K. Nagai, T. Iyoda, A. Yamada, T. Hayakawa, M. Ishiwara, S. Horaguchi, A. Belay, T. Tanaka, K. Takano, M. Hangyo, Spirulina-templated metal microcoils with controlled helical structures for THz electromagnetic responses, Sci. Rep. 4 (2014) 1–7, https://doi.org/10.1038/srep04919.

[33] X. Zhang, M. Yu, J. Liu, S. Li, Bioinspired synthesis of a hollow metallic microspiral based on a Spirulina bioscaffold, Langmuir. 28 (2012) 3690–3694, https://doi.org/10.1021/la204370x.

[34] D. Fu, D. Yuan, Spectrophotometric determination of trace copper in water samples with thiomichlersketone, Spectrochim. Acta - Part A Mol, Biomol. Spectrosc. 66 (2007) 434–437, https://doi.org/10.1016/j.saa.2006.03.018.

[35] H. Li, Z. Su, S. Hu, Y. Yan, Free-standing and flexible Cu/Cu2O/CuO heterojunction net: A novel material as cost-effective and easily recycled visible-light photocatalyst, Appl. Catal. B Environ. 207 (2017) 134–142, https://doi.org/10.1016/j.apcatb.2017.02.013.

[36] X. Jiang, T. Herricks, Y. Xia, CuO Nanowires Can Be Synthesized by Heating Copper Substrates in Air, Nano Lett. 2 (2002), https://doi.org/10.1021/nl0257519.

[37] M. Kaur, K.P. Muthe, S.K. Despande, S. Choudhury, J.B. Singh, N. Verma, S. K. Gupta, J.V. Yakhmi, Growth and branching of CuO nanowires by thermal oxidation of copper, J. Cryst. Growth. 289 (2006) 670–675, https://doi.org/10.1016/j.jcrysgro.2005.11.111.

[38] F. Zhang, S. Huang, Q. Guo, H. Zhang, H. Li, Y. Wang, J. Fu, X. Wu, L. Xu, M. Wang, One-step hydrothermal synthesis of Cu2O/CuO hollow microspheres/reduced graphene oxide hybrid with enhanced sensitivity for non-enzymatic glucose sensing, Colloids Surfaces A Physicochem. Eng. Asp. 602 (2020) 125076. doi:10.1016/j.colsurfa.2020.125076.

[39] D. Ranjith Kumar, D. Manoj, J. Santhanalakshmi, Optimization of site specific adsorption of oleylamine capped CuO nanoparticles on MWCNTs for electrochemical determination of guanosine, Sensors Actuators, B Chem. 188 (2013) 603–612, https://doi.org/10.1016/j.snb.2013.07.067.

[40] A. Al-Keisy, L. Ren, D. Cui, Z. Xu, X. Xu, X. Su, W. Hao, S.X. Dou, Y. Du, A ferroelectric photocatalyst Ag10Si4O13 with visible-light photooxidation properties, J. Mater. Chem. A. 4 (2016) 10992–10999, https://doi.org/10.1039/c6ta03578g.

[41] Y. Yang, D. Xu, Q. Wu, P. Diao, Cu2O/CuO bilayered composite as a high-efficiency photocathode for photoelectrochemical hydrogen evolution reaction, Sci. Rep. 6 (2016) 1–13, https://doi.org/10.1038/srep35158.

[42] A.A. Dubale, C.J. Pan, A.G. Tamirat, H.M. Chen, W.N. Su, C.H. Chen, J. Rick, D.W. Ayele, B.A. Aragaw, J.F. Lee, Y.W. Yang, B.J. Hwang, Heterostructured Cu2O/CuO decorated with nickel as a highly efficient photocathode for photoelectrochemical water reduction, J. Mater. Chem. A. 3 (2015) 12482–12499. doi:10.1039/c5ta01961c.

[43] X. Li, X. Yang, N. Wang, Y. Xie, Potential of Pteris vittata to Remove Tetracycline Antibiotics from Aquatic Media, Int. J. Phytoremediation. 17 (2015) 895–899, https://doi.org/10.1080/15226514.2014.989314.

[44] F. Chen, Q. Yang, J. Sun, F. Yao, S. Wang, Y. Wang, X. Wang, X. Li, C. Niu, D. Wang, G. Zeng, Enhanced Photocatalytic Degradation of Tetracycline by AgI/BiVO4 Heterojunction under Visible-Light Irradiation: Mineralization Efficiency and Mechanism, ACS Appl. Mater. Interfaces. 8 (2016) 32887–32900, https://doi.org/10.1021/acsami.6b12278.

[45] P. Punamiya, D. Sarkar, S. Rakshit, R. Datta, Effectiveness of Aluminum-based Drinking Water Treatment Residuals as a Novel Sorbent to Remove Tetracyclines from Aqueous Medium, J. Environ. Qual. 42 (2013) 1449–1459, https://doi.org/10.2134/jeq2013.03.0082.

[46] M. Liu, L. an Hou, S. Yu, B. Xi, Y. Zhao, X. Xia, MCM-41 impregnated with A zeolite precursor: Synthesis, characterization and tetracycline antibiotics removal from aqueous solution, Chem. Eng. J. 223 (2013) 678–687. doi:10.1016/j.cej.2013.02.088.

[47] L. Duan, L. Li, Z. Xu, W. Chen, Adsorption of tetracycline to nano-NiO: The effect of co-existing Cu(ii) ions and environmental implications, Environ. Sci. Process. Impacts. 16 (2014) 1462–1468, https://doi.org/10.1039/c4em00096j.

[48] D. a Palmer, P. Benezeth, Solubility of copper oxides in water and steam, 14Th Int. Conf. Prop. Water Steam Kyoto. (2008).

[49] C.K. Ko, W.G. Lee, Effects of pH variation in aqueous solutions on dissolution of copper oxide, Surf. Interface Anal. 42 (2010) 1128–1130, https://doi.org/10.1002/sia.3238.

[50] X. Wang, L. Jiang, K. Li, J. Wang, D. Fang, Y. Zhang, D. Tian, Z. Zhang, D. D. Dionysiou, Fabrication of novel Z-scheme SrTiO3/MnFe2O4 system with double-response activity for simultaneous microwave-induced and photocatalytic degradation of tetracycline and mechanism insight, Chem. Eng. J. 400 (2020), 125981, https://doi.org/10.1016/j.cej.2020.125981.

[51] W. Dai, L. Jiang, J. Wang, Y. Pu, Y. Zhu, Y. Wang, B. Xiao, Efficient and stable photocatalytic degradation of tetracycline wastewater by 3D Polyaniline/Perylene diimide organic heterojunction under visible light irradiation, Chem. Eng. J. 397 (2020), 125476, https://doi.org/10.1016/j.cej.2020.125476.

[52] Y. Pan, X. Yuan, L. Jiang, H. Wang, H. Yu, J. Zhang, Stable self-assembly AgI/UiO-66(NH2) heterojunction as efficient visible-light responsive photocatalyst for tetracycline degradation and mechanism insight, Chem. Eng. J. 384 (2020), 123310, https://doi.org/10.1016/j.cej.2019.123310.

[53] H. Wang, X. Yuan, Y. Wu, G. Zeng, H. Dong, X. Chen, L. Leng, Z. Wu, L. Peng, In situ synthesis of In2S3 at MIL-125(Ti) core-shell microparticle for the removal of tetracycline from wastewater by integrated adsorption and visible-light-driven photocatalysis, Appl. Catal. B Environ. 186 (2016) 19–29, https://doi.org/10.1016/j.apcatb.2015.12.041.

[54] P. Wang, P.S. Yap, T.T. Lim, C-N-S tridoped TiO2 for photocatalytic degradation of tetracycline under visible-light irradiation, Appl. Catal. A Gen. 399 (2011) 252–261, https://doi.org/10.1016/j.apcata.2011.04.008.

[55] Z. Xie, Y. Feng, F. Wang, D. Chen, Q. Zhang, Y. Zeng, W. Lv, G. Liu, Construction of carbon dots modified MoO3/g-C3N4 Z-scheme photocatalyst with enhanced visible-light photocatalytic activity for the degradation of tetracycline, Appl. Catal. B Environ. 229 (2018) 96–104, https://doi.org/10.1016/j.apcatb.2018.02.011.

[56] Y. Yang, Z. Zeng, C. Zhang, D. Huang, G. Zeng, R. Xiao, C. Lai, C. Zhou, H. Guo, W. Xue, M. Cheng, W. Wang, J. Wang, Construction of iodine vacancy-rich BiOI/Ag@AgI Z-scheme heterojunction photocatalysts for visible-light-driven tetracycline degradation: Transformation pathways and mechanism insight, Chem. Eng. J. 349 (2018) 808–821, https://doi.org/10.1016/j.cej.2018.05.093.

[57] B. Luo, D. Xu, D. Li, G. Wu, M. Wu, W. Shi, M. Chen, Fabrication of a Ag/Bi3TaO7 Plasmonic Photocatalyst with Enhanced Photocatalytic Activity for Degradation of Tetracycline, ACS Appl. Mater. Interfaces. 7 (2015) 17061–17069, https://doi.org/10.1021/acsami.5b03535.

[58] W. Shi, F. Guo, S. Yuan, In situ synthesis of Z-scheme Ag3PO4/CuBi2O4 photocatalysts and enhanced photocatalytic performance for the degradation of tetracycline under visible light irradiation, Appl. Catal. B Environ. 209 (2017) 720–728, https://doi.org/10.1016/j.apcatb.2017.03.048.

[59] F. Deng, L. Zhao, X. Luo, S. Luo, D.D. Dionysiou, Highly efficient visible-light photocatalytic performance of Ag/AgIn5S8 for degradation of tetracycline hydrochloride and treatment of real pharmaceutical industry wastewater, Chem. Eng. J. 333 (2018) 423–433, https://doi.org/10.1016/j.cej.2017.09.022.

[60] M. Ahmadi, H. Ramezani Motlagh, N. Jaafarzadeh, A. Mostoufi, R. Saeedi, G. Barzegar, S. Jorfi, Enhanced photocatalytic degradation of tetracycline and real pharmaceutical wastewater using MWCNT/TiO2 nano-composite, J. Environ. Manage. 186 (2017) 55–63, https://doi.org/10.1016/j.jenvman.2016.09.088.

[61] R. Yang, Z. Zhu, C. Hu, S. Zhong, L. Zhang, B. Liu, W. Wang, One-step preparation (3D/2D/2D) BiVO4/FeVO4@rGO heterojunction composite photocatalyst for the removal of tetracycline and hexavalent chromium ions in water, Chem. Eng. J. 390 (2020), 124522, https://doi.org/10.1016/j.cej.2020.124522.

[62] A.A. Dubale, A.G. Tamirat, H.M. Chen, T.A. Berhe, C.J. Pan, W.N. Su, B.J. Hwang, A highly stable CuS and CuS-Pt modified Cu2O/CuO heterostructure as an efficient photocathode for the hydrogen evolution reaction, J. Mater. Chem. A. 4 (2016) 2205–2216, https://doi.org/10.1039/c5ta09464j.

[63] A. Serrà, L. Philippe, Simple and scalable fabrication of hairy ZnO@ZnS core@shell Cu cables for continuous sunlight-driven photocatalytic water remediation, Chem. Eng. J. 401 (2020), 126164, https://doi.org/10.1016/j.cej.2020.126164.

[64] J. Han, X. Zong, X. Zhou, C. Li, Cu2O/CuO photocathode with improved stability for photoelectrochemical water reduction, RSC Adv. 5 (2015) 10790–10794, https://doi.org/10.1039/c4ra13896a.
[65] P.P. Kunturu, J. Huskens, Efficient Solar Water Splitting Photocathodes Comprising a Copper Oxide Heterostructure Protected by a Thin Carbon Layer, ACS Appl. Energy Mater. 2 (2019) 7850–7860, https://doi.org/10.1021/acsaem.9b01290.
[66] S. Jamali, A. Moshaii, Improving photo-stability and charge transport properties of Cu 2 O/CuO for photo-electrochemical water splitting using alternate layers of WO 3 or CuWO 4 produced by the same route, Appl. Surf. Sci. 419 (2017) 269–276, https://doi.org/10.1016/j.apsusc.2017.04.228.
[67] C.Y. Toe, J. Scott, R. Amal, Y.H. Ng, Recent advances in suppressing the photocorrosion of cuprous oxide for photocatalytic and photoelectrochemical energy conversion, J. Photochem. Photobiol. C Photochem. Rev. 40 (2019) 191–211, https://doi.org/10.1016/j.jphotochemrev.2018.10.001.